The IRM Quarterly
Winter 2015, Vol. 25 No.4
ISSN: 2152-1972

Inside...

Adding Geochemistry to the IRM Toolkit:
Acquisition of a Portable X-ray Fluorescence Spectrometer

Ellery Frahm[1] and Joshua Feinberg[2]
[1]Anthropology Department, University of Minnesota
[2]Institute for Rock Magnetism

Ellery Frahm using the IRM's new portable X-ray fluorescence instrument at an archaeological site in Armenia.

The IRM continues to add to the analytical techniques and instruments available to visiting fellows and other researchers: the latest addition is the non-destructive elemental analysis by portable X-ray fluorescence spectrometry (pXRF). Much of the research at the IRM aims to quantify the composition, concentration, and grain size distribution of Fe-bearing minerals in natural and synthetic samples. Whether we measure the rock magnetic properties of igneous, sedimentary, metamorphic, or even extraterrestrial environments, complementary geochemical information about our specimens can often improve the accuracy of our geophysical interpretations. Recent improvements in the calibration, safety, and sensitivity of pXRF devices has led to a rapid expansion of their use in a number of fields, including sedimentology and stratigraphy (Funk et al., 2004a,b; Lami et al., 2004; Luterbacher et al., 2004; Rohl et al., 2004; Meijers et al., 2016), economic geology (Gazley et al., 2015), soil science (Martin Peinado et al., 2010), environmental remediation (Jamieson et al., 2015), and archaeology and anthropology (Frahm et al., 2014a,b, 2016). In short, there are many innovative ways in which this instrument can serve future visitors to the IRM.

The pXRF is a hand-held instrument the size of a small portable drill that allows one to identify and quantify approximately 50 elements ranging in atomic weight from Mg to U. Analyses can be conducted in the field, with data being digitally recorded and geo-referenced instantaneously, or in the quiet and coziness of IRM where the pXRF can be conveniently rested on a stand, making measurements more systematic.

Motivation to acquire the pXRF arose from the research of Dr. Ellery Frahm during his postdoctoral work at the IRM. Ellery characterizes obsidian artifacts from archaeological sites and volcanic terranes and has made pXRF a fundamental component of his research (e.g., Frahm et al., 2014a,b, 2016; Adler et al., 2014).

How it Works

When a material is exposed to high-energy (short-wavelength) X-rays, a portion of its constituent atoms may ionize (i.e., one or more orbital electrons are ejected from an atom). Sufficiently energetic X-rays can trigger the ejection of electrons from inner orbitals: when an electron from a higher orbital "falls" into the vacancy left in the inner orbital, it will emit a photon that lies in the X-ray portion of the electromagnetic spectrum and is characteristic of the element involved. These photons can be sorted by either their energies (which is termed energy-dispersive XRF or ED-XRF) or their wavelengths (wavelength-dispersive XRF or WD-XRF) and allow the identification of the elements present. In each

cont'd. on pg. 9...

Visiting Fellow Report

Mudrock fabric using high field magnetic anisotropy

Josep M. Pares
Paleomagnetism Laboratory, CENIEH, Paseo Sierra de Atapuerca 3, 09002-Burgos, Spain

josep.pares@cenieh.es

Rock fabrics are fundamental in earth sciences as they determine numerous physical properties such as seismic anisotropy, fracture development, permeability and fluid circulation, and therefore understanding and characterizing rock fabrics is critical in geosciences.

The anisotropy of magnetic susceptibility (AMS) has been established in the past thirty years as the most versatile, sensitive, and rapid proxy for rock fabrics characterization. Standard measurements of the magnetic anisotropy involve the low-field AMS, which responds to the bulk of the mineralogy of the rock sample, including the paramagnetic, ferromagnetic, and diamagnetic fractions. Separation methods of para- and ferromagnetic anisotropies (K_{para} and K_{ferr}) have progressively gained interest over the last thirty years, including mathematical and instrumental approaches (e.g., Martín-Hernández and Ferré, 2007), and basically they involve the use of either a torque magnetometer or a vibrating sample magnetometer (VSM). The so-called anisotropy of high field magnetic susceptibility (AHFMS, Bilardello and Jackson, 2014) using a Vibrating Sample Magnetometer (VSM) is a very powerful tool to discriminate K_{ferr} from K_{para} tensors. Nevertheless, the method has almost exclusively been used in crystalline, highly magnetic or anisotropic rocks (e.g., granulites- Bilardello and Jackson, 2014; migmatites- Ferré et al., 2004, metagreywackes and slates- Kelso et al., 2002; peridotites- Martín-Hernández and Ferré, 2007). Much less is known as far as the AHFMS in weakly deformed sedimentary rocks with feeble magnetic anisotropy (<5%). Can we also separate the K_{para} from K_{ferr} tensors in these rocks where both bulk susceptibility and degree of anisotropy are much lower?

Fabric separation could help to elucidate the deformation mechanism that produces magnetic tectonic fabric in mudrocks: Because phyllosilicates (K_{para}) appear as platy grains whereas magnetite (K_{ferr}) typically as euhedral, it is critical to separately characterize their preferred orientation and degree of alignment, due to their contrasting rheology upon stress. Intrigued by the role of paramagnetic versus ferromagnetic components in these weakly deformed rocks, we aimed at extending the application of AHFMS to mudrocks that according to the standard AMS have embryonic deformation.

The method for subfabric separation based on high-field measurement with a VSM was developed by Ferré et al. (2000) and Kelso et al. (2002). The principle of VSM analysis is based on the flux change in the pick-up coil system produced by vibrating a sample (rather than by rotation, as in spinner magnetometers). Although primarily designed for the measurement of hysteresis properties, there have been successful attempts to use VSM's to obtain directional hysteresis curves along different orientations of the specimen, hence enabling to the calculation of the high field magnetic anisotropy, which is the purpose of our study.

Some important issues to consider when determining the AHFMS with a VSM include: (1) the thermal equilibrium of the sample with the pole gap space is critical; (2) sample should be centered within the pole gap; (3) cubic specimens seem to produce better results than standard cylinders.

We selected a number of mudrock and fine grain sandstone specimens (1.1 cm^3) to measure with the Princeton Measurements Micromag VSM at the IRM. The cubic specimens were carefully well centered within the pole gap- critical for the measurements, and the plastic sample holder was modified by Peat Solheid (IRM) during the visit to reduce the background, diamagnetic noise. The configuration for the measurements was: (1) 1 T maximum field; (2) 0.2 s averaging time for each measurement; (3) 5 mT field increment between measurements; (4) 30º rotation increment between loops. We therefore measured a total of 36 hysteresis curves per specimen (e.g., Bilardello and Jackon, 2014) as opposed to 24 (e.g., Ferré et al., 2004), which largely improve results. Each hysteresis loop (12 per axis) was repeated three times on some pilot samples, although the majority of them was measured once, dramatically reducing the total measuring time to about one hour and a half per specimen. Special care was taken in leaving the specimens within the pole gap for about 20 minutes previous to the measurements, for a uniform temperature (e.g., Kelso et al., 2002).

Figure 1 shows the results for some Eocene mudrocks from the Southern Pyrenean Foreland Basin. Anisotropy of Magnetic Susceptibility was measured on a MFK1-FA, with a field of 200 Am^{-1}, at an operating frequency of 976 Hz. Magnetic ellipsoids are oblate (average T = 0.66), and with an average anisotropy degree of 1.044. Principal axes distribution reveals a subvertical K_{min}, which is perpendicular to bedding. K_{max} axes are thought to reflect the intersection between the E-W direction flattening plane and sub-horizontal (<5º) bedding. Such intermediate fabric has been widely observed in the Pyrenean foreland basin and in active accretionary prisms (Parés, 2015). The anisotropy of high magnetic susceptibility (AHFMS) was calculated from the high-field slopes obtained in the Micromag VSM. The degree of the high field anisotropy is 10% (Pj=1.10 on average), and the axes distribution is somewhat more intriguing than those of the AMS: Whereas the minimum axes of the AHFMS tend to be sub-vertical and hence around the pole to bedding, the maximum axes are scattered within bedding, almost defining a mean magnetic lineation about a NNE-SSW direction. Comparison of both AMS

and AHFMS axes distribution suggests switching of the maximum and intermediate axes of AHFMS (and of low DC field susceptibility, ADCMS). AHFMS axes permutation relative to those of AMS possibly reflects that the former suffers from incomplete saturation, which can lead to either inverted or misaligned fabrics (e.g., Bilardello and Jackson, 2014). Further investigation will be required to illuminate such axes switching.

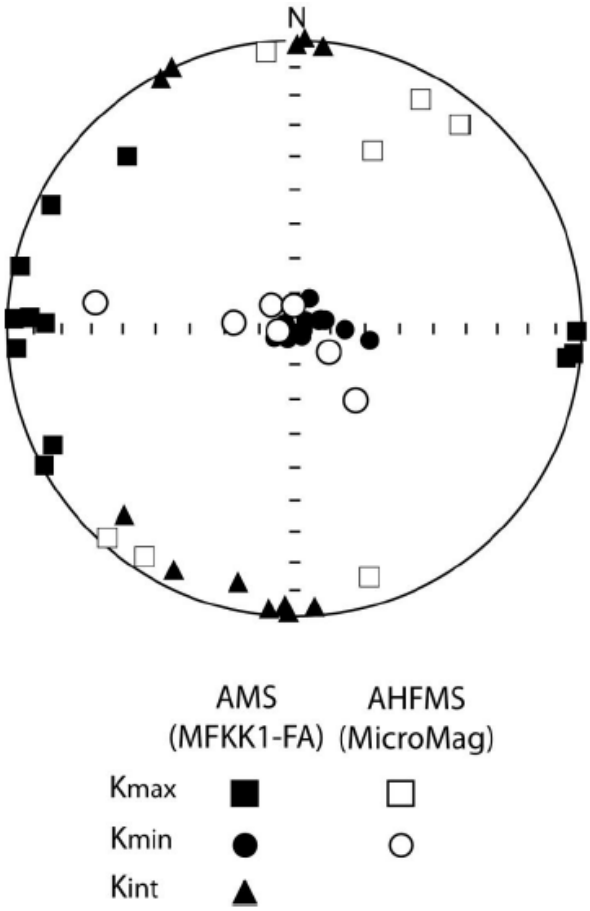

Figure 1. Figure 1: Magnetic fabrics measured for some Eocene mudrocks from the Pyrenean Foreland Basin. Closed symbols show the principal susceptibility axes obtained from the measurement of the low-field anisotropy of magnetic susceptibility (AMS). Open symbols are the axes (only Kmax and Kmin are represented) of the anisotropy of high field magnetic susceptibility (AHFMS)

Mike Jackson was very kind to add few modifications in "real time" to the "Princeton Ferret Software" to facilitate data evaluation and quality assessment, including the possibility to visualize the induced magnetization versus orientation (Fig. 2). The variation of magnetization as a function of orientation should have a π response, as every 7th hysteresis cycle is measured along the same axis. On the other hand, apparent anisotropy due to the shape effect of the measured cubes (e.g., Kelso et al., 2002) would have a π/2 term (i.e., along the corners), which is not observed in our samples. This result indicates that the sample shape effects are minimal and that the directional variability in magnetization mostly responds to the anisotropy of the sample.

Our pilot study showed that although much weaker than in crystalline rocks, the high field magnetic susceptibility anisotropy can be obtained with the Micromag VSM in mudrocks and sandstones, although several aspects do need further research: (i) Comparing cylindrical versus cubic samples, (ii) reducing the mass of the holders, (iii) changing pole spacing to gain field uniformity within the pole gap of the magnetometer, (iv) origin of axes permutation.

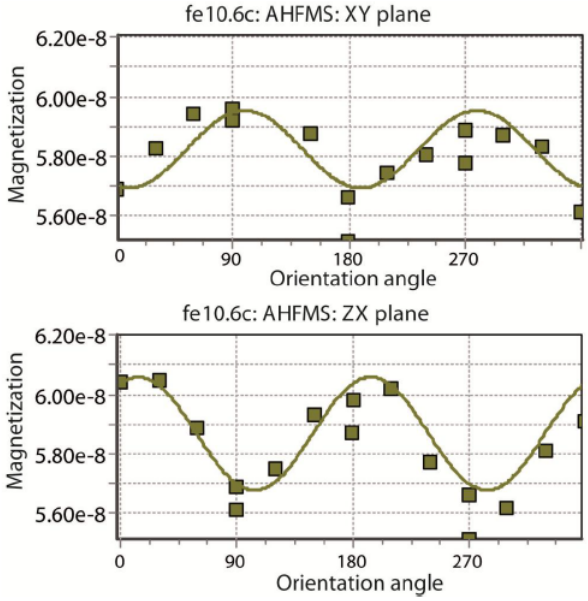

Figure 2. Example of the variation of magnetic moment with sample orientation (XY and ZX planes). Notice the π response of the magnetization (solid lines).

Acknowledgements

We thank the Review and Advisory Committee for supporting the IRM Visiting Fellowship. We are also indebted to Mike Jackson, Dario Bilardello, and Peter Solheid from the IRM for their assistance, patience, and hospitality during the visit.

References

Bilardello, D. and Jackson, M.J., 2014. A comparative study of magnetic anisotropy measurement techniques in relation to rock-magnetic properties.Tectonophysics, 629: 39-54.

Ferré, E.C. and Ameglio, L. 2000. Preserved magnetic fabrics vs. annealed microstructures in the syntectonic recrystallised George granite, South Africa. Jour. Struct. Geol., 22, 1199-1219.

Ferre, E.C.; Martín-Hernández, F.; Teyssier, C. and Jackson, M., 2004. Paramagnetic and ferromagnetic anisotropy of magnetic susceptibility in migmatites: measurements in high and low fields and kinematic implications. Geophys. J. Int., 157: 1119-1129.

Kelso, P., Tikoff, B., Jackson, M. & Sun, W., 2002. A new method for the separation of paramagnetic and ferromagnetic susceptibility anisotropy using low field and high field methods, Geophys. J. Int., 151, 345–359.

Martín-Hernández, F. and Ferré, E.C. 2007. Separation of paramagnetic and ferrimagnetic anisotropies, J. Geophys. Res., 112(B3), doi: 10.1029 / 2006JB004340.

Parés, J.M., 2015. Sixty Years of Anisotropy of Magnetic Susceptibility in deformed sedimentary rocks, Front. Earth Sci. 3:4. doi: 10.3389/feart.2015.00004.

Current Articles

A list of current research articles dealing with various topics in the physics and chemistry of magnetism is a regular feature of the IRM Quarterly. Articles published in familiar geology and geophysics journals are included; special emphasis is given to current articles from physics, chemistry, and materials-science journals. Most are taken from ISI Web of Knowledge, after which they are subjected to Procrustean culling for this newsletter. An extensive reference list of articles (primarily about rock magnetism, the physics and chemistry of magnetism, and some paleomagnetism) is continually updated at the IRM. This list, with more than 10,000 references, is available free of charge. Your contributions both to the list and to the Current Articles section of the IRM Quarterly are always welcome.

Archeomagnetism

Arnold, L. J., and M. Demuro (2015), Insights into TT-OSL signal stability from single-grain analyses of known-age deposits at Atapuerca, Spain, Quaternary Geochronology, 30, 472-478.

Arzarello, M., L. De Weyer, and C. Peretto (2016), The first European peopling and the Italian case: Peculiarities and "opportunism", Quaternary International, 393, 41-50.

Ellenblum, R., S. Marco, R. Kool, U. Davidovitch, R. Porat, and A. Agnon (2015), Archaeological record of earthquake ruptures in Tell Ateret, the Dead Sea Fault, Tectonics, 34(10), 2105-2117.

Ertepinar, P., C. G. Langereis, A. J. Biggin, L. V. de Groot, F. Kulakoglu, S. Omura, and A. Suel (2016), Full vector archaeomagnetic records from Anatolia between 2400 and 1350 BCE: Implications for geomagnetic field models and the dating of fires in antiquity, Earth and Planetary Science Letters, 434, 171-186.

Frahm, E., J. M. Feinberg, B. A. Schmidt-Magee, K. N. Wilkinson, B. Gasparyan, B. Yeritsyan, and D. S. Adler (2016), Middle Palaeolithic toolstone procurement behaviors at Lusakert Cave 1, Hrazdan valley, Armenia, Journal of Human Evolution, 91, 73-92.

Gibert, L., G. R. Scott, D. Scholz, A. Budsky, C. Ferrandez, F. Ribot, R. A. Martin, and M. Leria (2016), Chronology for the Cueva Victoria fossil site (SE Spain): Evidence for Early Pleistocene Afro-Iberian dispersals, Journal of Human Evolution, 90, 183-197.

Kostadinova-Avramova, M., and M. Kovacheva (2015), Further studies on the problems of geomagnetic field intensity determination from archaeological baked clay materials, Geophysical Journal International, 203(1), 588-604.

Le Tensorer, J. M., H. Le Tensorer, P. Martini, V. von Falkenstein, P. Schmid, and J. J. Villalain (2015), The Oldowan site Ain al Fil (El Kowm, Syria) and the first humans of the Syrian Desert, Anthropologie, 119(5), 581-594.

Mosquera, M., P. Saladie, A. Olle, I. Caceres, R. Huguet, J. J. Villalain, A. Carrancho, D. Bourles, R. Braucher, and J. Vallverdu (2015), Barranc de la Boella (Catalonia, Spain): an Acheulean elephant butchering site from the European late Early Pleistocene, Journal of Quaternary Science, 30(7), 651-666.

Rouzeau, B., A. Genevey, Y. Gallet, and M. Le Goff (2015), New Constraints on the Metallurgical Activity at the Morimond Abbey (Haute-Marne) from the Archeomagnetic Analysis of two Excavated Brick Fireplaces, Archeosciences-Revue D Archeometrie(39), 39-49.

Tema, E., E. Zanella, F. J. Pavon-Carrasco, D. Kondopoulou, and S. Pavlides (2015), Palaeomagnetic analysis on pottery as indicator of the pyroclastic flow deposits temperature: new data and statistical interpretation from the Minoan eruption of Santorini, Greece, Geophysical Journal International, 203(1), 33-47.

Tema, E., G. Polymeris, J. Morales, A. Goguitchaichvili, and V. Tsaknaki (2015), Dating of ancient kilns: A combined archaeomagnetic and thermoluminescence analysis applied to a brick workshop at Kato Achaia, Greece, Journal of Cultural Heritage, 16(4), 496-507.

Biomagnetism

Jozefczak, A., B. Leszczynski, A. Skumiel, and T. Hornowski (2016), A comparison between acoustic properties and heat effects in biogenic (magnetosomes) and abiotic magnetite nanoparticle suspensions, Journal of Magnetism and Magnetic Materials, 407, 92-100.

Kishkinev, D. (2015), Sensory mechanisms of long-distance navigation in birds: a recent advance in the context of previous studies, Journal of Ornithology, 156, S145-S161.

Kolinko, S., M. Richter, F. O. Glockner, A. Brachmann, and D. Schuler (2016), Single-cell genomics of uncultivated deep-branching magnetotactic bacteria reveals a conserved set of magnetosome genes, Environmental Microbiology, 18(1), 21-37.

Manrique-Julio, J., F. Machuca-Martinez, N. Marriaga-Cabrales, and M. Pinzon-Cardenas (2016), Production of magnetite by electrolytic reduction of ferric oxyhydroxide, Journal of Magnetism and Magnetic Materials, 401, 81-85.

Mathuriya, A. S., K. Yadav, and B. D. Kaushik (2015), Magnetotactic Bacteria: Performances and Challenges, Geomicrobiology Journal, 32(9), 780-788.

Miranda, A. G. C., M. A. E. Chaparro, and H. N. Bohnel (2016), Magnetic properties of Tillandsia recurvata L. and its use for biomonitoring a Mexican metropolitan area, Ecological Indicators, 60, 125-136.

Pan, W. D., G. J. Wan, J. J. Xu, X. M. Li, Y. X. Liu, L. P. Qi, and F. J. Chen (2016), Evidence for the presence of biogenic magnetic particles in the nocturnal migratory brown planthopper, Nilaparvata lugens, Scientific Reports, 6.

Petryshyn, V. A., F. A. Corsetti, C. M. Frantz, S. P. Lund, and W. M. Berelson (2016), Magnetic susceptibility as a biosignature in stromatolites, Earth and Planetary Science Letters, 437, 66-75.

Zhao, X. Y., R. Egli, S. A. Gilder, and S. Muller (2016), Microbially assisted recording of the Earth's magnetic field in sediment, Nature Communications, 7.

Environmental magnetism and Climate

Abadi, M. S., A. C. Da Silva, H. Mossadegh, S. Spassov, and F. Boulvain (2015), Lower Carboniferous ramp sedimentation of the Central Alborz Basin, northern Iran: integrated sedimentological and rock-magnetic studies, in Magnetic Susceptibility Application: A Window onto Ancient Environments and Climatic Variations, edited by A. C. DaSilva, M. T. Whalen, J. Hladil, L. Chadimova, D. Chen, S. Spassov, F. Boulvain and X. Devleeschouwer, pp. 73-91.

Altin, T. B., M. El Ouahabi, and N. Fagel (2015), Environmental and climatic changes during the Pleistocene-Holocene in the Bor Plain, Central Anatolia, Turkey, Palaeogeography Palaeoclimatology Palaeoecology, 440, 564-578.

Avinash, K., P. J. Kurian, A. K. Warrier, R. Shankar, T. C. Vineesh, and R. Ravindra (2016), Sedimentary sources and processes in the eastern Arabian Sea: Insights from environmental magnetism, geochemistry and clay mineralogy, Geoscience Frontiers, 7(2), 253-264.

Cao, L. W., E. Appel, W. Rosler, and T. Magiera (2015), Efficiency of stepwise magnetic-chemical site assessment for fly ash derived heavy metal pollution, Geophysical Journal International, 203(2), 767-775.

Cerny, J., M. T. Ramirez-Herrera, M. F. Bogalo, A. Goguitchaichvili, R. Castillo-Aja, J. Morales, J. A. Sanchez-Cabeza, and A. Ruiz-Fernandez (2016), Magnetic record of extreme marine inundation events at Las Salinas site, Jalisco, Mexican Pacific coast, International Geology Review, 58(3), 342-357.

Chadimova, L., F. Vacek, K. Sobien, L. Slavik, and J. Hladil (2015), Petrophysical record of the Late Silurian shallow-water carbonate facies across the Lau Event (Prague Synform, Czech Republic) and dynamic time warping alignment of the magnetic susceptibility logs, in Magnetic Susceptibility Application: A Window onto Ancient Environments and Climatic Variations, edited by A. C. DaSilva, M. T. Whalen, J. Hladil, L. Chadimova, D. Chen, S. Spassov, F. Boulvain and X. Devleeschouwer, pp. 133-155.

Channell, J. E. T., D. A. Hodell, and J. H. Curtis (2016), Relative paleointensity (RPI) and oxygen isotope stratigraphy at IODP Site U1308: North Atlantic RPI stack for 1.2-2.2 Ma (NARPI-2200) and age of the Olduvai Subchron, Quaternary Science Reviews, 131, 1-19.

Civeira, M. S., R. N. Pinheiro, A. Gredilla, S. F. O. de Vallejuelo, M. L. S. Oliveira, C. G. Ramos, S. R. Taffarel, R. M. Kautzmann, J. M. Madariaga, and L. F. O. Silva (2016), The properties of the nanominerals and hazardous elements: Potential environmental impacts

of Brazilian coal waste fire, Science of the Total Environment, 544, 892-900.

Da Silva, A. C., M. T. Whalen, J. Hladil, L. Chadimova, D. Chen, S. Spassov, F. Boulvain, and X. Devleeschouwer (2015), Magnetic susceptibility application: a window onto ancient environments and climatic variations: foreword, in Magnetic Susceptibility Application: A Window onto Ancient Environments and Climatic Variations, edited by A. C. DaSilva, M. T. Whalen, J. Hladil, L. Chadimova, D. Chen, S. Spassov, F. Boulvain and X. Devleeschouwer, pp. 1-13.

Dallanave, E., V. Bachtadse, E. M. Crouch, L. Tauxe, C. L. Shepherd, H. E. G. Morgans, C. J. Hollis, B. R. Hines, and S. Sugisaki (2016), Constraining early to middle Eocene climate evolution of the southwest Pacific and Southern Ocean, Earth and Planetary Science Letters, 433, 380-392.

Dalmora, A. C., C. G. Ramos, X. Querol, R. M. Kautzmann, M. L. S. Oliveira, S. R. Taffarela, T. Moreno, and L. F. O. Silva (2016), Nanoparticulate mineral matter from basalt dust wastes, Chemosphere, 144, 2013-2017.

Devleeschouwer, X., L. Riquier, O. Babek, D. De Vleeshouwer, E. Petitclerc, S. Sterckx, and S. Spassov (2015), Magnetization carriers of grey to red deep-water limestones in the GSSP of the Givetian-Frasnian boundary (Puech de la Suque, France): signals influenced by moderate diagenetic overprinting, in Magnetic Susceptibility Application: A Window onto Ancient Environments and Climatic Variations, edited by A. C. DaSilva, M. T. Whalen, J. Hladil, L. Chadimova, D. Chen, S. Spassov, F. Boulvain and X. Devleeschouwer, pp. 157-180.

Ellwood, B. B., A. El Hassani, J. H. Tomkin, and P. Bultynck (2015), A climate-driven model using time-series analysis of magnetic susceptibility (chi) datasets to represent a floating-point high-resolution geological timescale for the Middle Devonian Eifelian stage, in Magnetic Susceptibility Application: A Window onto Ancient Environments and Climatic Variations, edited by A. C. DaSilva, M. T. Whalen, J. Hladil, L. Chadimova, D. Chen, S. Spassov, F. Boulvain and X. Devleeschouwer, pp. 209-223.

Font, E., J. Ponte, T. Adatte, A. Fantasia, F. Florindo, A. Abrajevitch, and J. Mirao (2016), Tracing acidification induced by Deccan Phase 2 volcanism, Palaeogeography Palaeoclimatology Palaeoecology, 441, 181-197.

Gorka-Kostrubiec, B., M. Teisseyre-Jelenska, and S. K. Dytlow (2016), Magnetic properties as indicators of Chernozem soil development, Catena, 138, 91-102.

Grabowski, J., M. Narkiewicz, and D. De Vleeschouwer (2015), Forcing factors of the magnetic susceptibility signal in lagoonal and subtidal depositional cycles from the Zachelmie section (Eifelian, Holy Cross Mountains, Poland), in Magnetic Susceptibility Application: A Window onto Ancient Environments and Climatic Variations, edited by A. C. DaSilva, M. T. Whalen, J. Hladil, L. Chadimova, D. Chen, S. Spassov, F. Boulvain and X. Devleeschouwer, pp. 225-244.

Grison, H., E. Petrovsky, A. Kapicka, and S. Stejskalova (2016), Magnetic and chemical parameters of andic soils and their relation to selected pedogenesis factors, Catena, 139, 179-190.

Guo, X. L., X. M. Liu, S. J. Miao, G. Y. Zhao, and Y. X. Liu (2015), Variability of magnetic character of S5-1 paleosol (age similar to 470 Ka) along a rainfall transect explains why susceptibility decreased with high rainfall, Aeolian Research, 19, 55-63.

Haliuc, A., S. M. Hutchinson, G. Florescu, and A. Feurdean (2016), The role of fire in landscape dynamics: An example of two sediment records from the Rodna Mountains, northern Romanian Carpathians, Catena, 137, 432-440.

Henkel, S., S. Kasten, S. W. Poulton, and M. Staubwasser (2016), Determination of the stable iron isotopic composition of sequentially leached iron phases in marine sediments, Chemical Geology, 421, 93-102.

Hesse, R. (2016), Ice-proximal Labrador Sea Heinrich layers: a sedimentological approach, Canadian Journal of Earth Sciences, 53(1), 71-100.

Howard, J. L., and K. M. Orlicki (2015), Effects of Anthropogenic Particles on the Chemical and Geophysical Properties of Urban Soils, Detroit, Michigan, Soil Science, 180(4-5), 154-166.

Howard, J. L., and K. M. Orlicki (2016), Composition, micromorphology and distribution of microartifacts in anthropogenic soils, Detroit, Michigan, USA, Catena, 138, 103-116.

Jadot, H., and F. Boulvain (2015), Sedimentology and magnetic susceptibility of recent sediments from New Caledonia, in Magnetic Susceptibility Application: A Window onto Ancient Environments and Climatic Variations, edited by A. C. DaSilva, M. T. Whalen, J. Hladil, L. Chadimova, D. Chen, S. Spassov, F. Boulvain and X. Devleeschouwer, pp. 111-132.

Jordanova, N., D. Jordanova, and P. Petrov (2016), Soil magnetic properties in Bulgaria at a national scale-Challenges and benefits, Global and Planetary Change, 137, 107-122.

Kettanah, Y. A., A. J. Mory, G. D. Wach, and M. T. D. Wingate (2015), Provenance of the Ordovician-lower Silurian Tumblagooda Sandstone, Western Australia, Australian Journal of Earth Sciences, 62(7), 817-830.

Lanci, L., and A. M. Hirt (2015), Evidence of Atlantic Multidecadal Oscillation in the magnetic properties of Alpine lakes during the last 2500 years, Palaeogeography Palaeoclimatology Palaeoecology, 440, 47-52.

Li, G. H., D. S. Xia, J. Jia, S. Zhao, F. Y. Gao, Y. J. Wang, H. Lu, and F. H. Chen (2015), Magnetic properties derived from a loess section at the northern piedmont of Tianshan Mountains, Xinjiang, China, and their paleoenvironmental significance, Geophysical Journal International, 203(2), 828-839.

Liu, D. X., J. H. Ma, Y. L. Sun, and Y. M. Li (2016), Spatial distribution of soil magnetic susceptibility and correlation with heavy metal pollution in Kaifeng City, China, Catena, 139, 53-60.

Lu, S. G., X. L. Yu, and Y. Y. Chen (2016), Magnetic properties, microstructure and mineralogical phases of technogenic magnetic particles (TMPs) in urban soils: Their source identification and environmental implications, Science of the Total Environment, 543, 239-247.

Macphail, M., L. K. Fifield, B. Pillans, M. Davies, and G. Hope (2015), Lake George revisited: New evidence for the origin and evolution of a large closed lake, Southern Tablelands, NSW, Australia, Australian Journal of Earth Sciences, 62(7), 853-871.

Martins, V., et al. (2016), Factors controlling air quality in different European subway systems, Environmental Research, 146, 35-46.

Mei, X., R. H. Li, X. H. Zhang, Q. S. Liu, J. X. Liu, Z. B. Wang, X. H. Lan, J. Liu, and R. T. Sun (2016), Evolution of the Yellow Sea Warm Current and the Yellow Sea Cold Water Mass since the Middle Pleistocene, Palaeogeography Palaeoclimatology Palaeoecology, 442, 48-60.

Morales, J., M. D. Hernandez-Bernal, P. Corona-Chavez, A. Gogichaishvili, and F. Bautista (2016), Further evidence for magnetic susceptibility as a proxy for the evaluation of heavy metals in mining wastes: case study of Tlalpujahua and El Oro Mining Districts, Environmental Earth Sciences, 75(4).

Pal, S. K., J. Vaish, S. Kumar, and A. K. Bharti (2016), Coal fire mapping of East Basuria Colliery, Jharia coalfield using vertical derivative technique of magnetic data, Journal of Earth System Science, 125(1), 165-178.

Pellegrini, S., G. Garcia, J. M. Penas-Castejon, N. Vignozzi, and E. A. C. Costantini (2016), Pedogenesis in mine tails affects macroporosity, hydrological properties, and pollutant flow, Catena, 136, 3-16.

Rabeh, T. (2016), Tracing the manganese ore accumulations in Sinai Peninsula, Egypt, using magnetic method, Environmental Earth Sciences, 75(3).

Rawat, S., A. K. Gupta, P. Srivastava, S. J. Sangode, and H. C. Nainwal (2015), A 13,000 year record of environmental magnetic variations in the lake and peat deposits from the Chandra valley, Lahaul: Implications to Holocene monsoonal variability in the NW Himalaya, Palaeogeography Palaeoclimatology Palaeoecology, 440, 116-127.

Roberts, A. P. (2015), Magnetic mineral diagenesis, Earth-Science Reviews, 151, 1-47.

Saarni, S., T. Saarinen, and P. Dulski (2016), Between the North Atlantic Oscillation and the Siberian High: A 4000-year snow accumulation history inferred from varved lake sediments in Finland, Holocene, 26(3), 423-431.

Savian, J. F., L. Jovane, M. Giorgioni, F. Iacoviello, D. Rodelli, A. P. Roberts, L. Chang, F. Florindo, and M. Sprovieri (2016), Environmental magnetic implications of magnetofossil occurrence during the Middle Eocene Climatic Optimum (MECO) in pelagic sediments from the equatorial Indian Ocean, Palaeogeography Palaeoclimatology Palaeoecology, 441, 212-222.

Suk, D. (2016), Environmental conditions for the presence of mag-

netofossils in the Last Glacial Maximum inferred from magnetic parameters of sediments from the Ulleung Basin, East Sea, Marine Geology, 372, 53-65.
Sun, Z. X., P. R. Owens, C. L. Han, H. Chen, X. L. Wang, and Q. B. Wang (2016), A quantitative reconstruction of a loess-paleosol sequence focused on paleosol genesis: An example from a section at Chaoyang, China, Geoderma, 266, 25-39.
Wang, Y., J. J. Jiao, K. Zhang, and Y. Z. Zhou (2016), Enrichment and mechanisms of heavy metal mobility in a coastal quaternary groundwater system of the Pearl River Delta, China, Science of the Total Environment, 545, 493-502.
Wang, B., D. S. Xia, Y. Yu, J. Jia, Y. Nie, and X. Wang (2015), Detecting the sensitivity of magnetic response on different pollution sources - A case study from typical mining cities in northwestern China, Environmental Pollution, 207, 288-298.
Wu, Y., Z. Y. Zhu, S. F. Qiu, Y. L. Han, J. X. Cai, and Z. G. Rao (2016), Magnetic stratigraphy constraints on the Matuyama-Brunhes boundary recorded in a loess section at the southern margin of Chinese Loess Plateau, Geophysical Journal International, 204(2), 1072-1085.
Xiao, W. S., T. Frederichs, R. Gersonde, G. Kuhn, O. Esper, and X. Zhang (2016), Constraining the dating of late Quaternary marine sediment records from the Scotia Sea (Southern Ocean), Quaternary Geochronology, 31, 97-118.

Extraterrestiram and Planetary Magnetism

Collareta, A., M. D'Orazio, M. Gemelli, A. Pack, and L. Folco (2016), High crustal diversity preserved in the lunar meteorite Mount DeWitt 12007 (Victoria Land, Antarctica), Meteoritics & Planetary Science, 51(2), 351-371.
Connerney, J. E. P., J. R. Espley, G. A. DiBraccio, J. R. Gruesbeck, R. J. Oliversen, D. L. Mitchell, J. Halekas, C. Mazelle, D. Brain, and B. M. Jakosky (2015), First results of the MAVEN magnetic field investigation, Geophysical Research Letters, 42(21), 8819-8827.
Isac, A., M. Mandea, M. Purucker, and B. Langlais (2016), A comparative analysis of the magnetic field signals over impact structures on the Earth, Mars and the Moon, Advances in Space Research, 57(1), 477-492.

Fundamental Rock and Mineral Magnetism

Berndt, T., A. R. Muxworthy, and G. A. Paterson (2015), Determining themagnetic attempt time tau(0), its temperature dependence, and the grain size distribution from magnetic viscosity measurements, Journal of Geophysical Research-Solid Earth, 120(11), 7322-7336.
Bykova, E., et al. (2016), Structural complexity of simple Fe2O3 at high pressures and temperatures, Nature Communications, 7.
Crider, J. G., D. M. Globokar, R. F. Burmester, and B. A. Housen (2015), Unblocking temperatures of viscous remanent magnetism in displaced granitic boulders, Icicle Creek glacial moraines (Washington, USA), Geophysical Research Letters, 42(24).
Cubukcu, H. E. (2015), Vertical variation in the deuteric oxidation of titanomagnetites in an ignimbrite deposit: Kizilkaya Ignimbrite (Cappadocia, Turkey), Journal of Volcanology and Geothermal Research, 308, 10-18.
Cuenca, J. A., K. Bugler, S. Taylor, D. Morgan, P. Williams, J. Bauer, and A. Porch (2016), Study of the magnetite to maghemite transition using microwave permittivity and permeability measurements, Journal of Physics-Condensed Matter, 28(10).
Dubrovskiy, A. A., D. A. Balaev, K. A. Shaykhutdinov, O. A. Bayukov, O. N. Pletnev, S. S. Yakushkin, G. A. Bukhtiyarova, and O. N. Martyanov (2015), Size effects in the magnetic properties of epsilon-Fe2O3 nanoparticles, Journal of Applied Physics, 118(21).
Dunlop, D. J. (2015), Transition warming and cooling remanences in pyrrhotite and hematite, Geophysical Journal International, 203(1), 605-613.
Evans, B. W., W. Hildreth, O. Bachmann, and B. Scaillet (2016), In defense of magnetite-ilmenite thermometry in the Bishop Tuff and its implication for gradients in silicic magma reservoirs, American Mineralogist, 100(1-2), 469-482.
Harres, A., M. Mikhov, V. Skumryev, A. M. H. de Andrade, J. E. Schmidt, and J. Geshev (2016), Criteria for saturated magnetization loop, Journal of Magnetism and Magnetic Materials, 402, 76-82.
Koulialias, D., J. Kind, M. Charilaou, P. G. Weidler, J. F. Loffler, and A. U. Gehring (2016), Variable defect structures cause the magnetic low-temperature transition in natural monoclinic pyrrhotite, Geophysical Journal International, 204(2), 961-967.
Randi, F., et al. (2016), Phase separation in the nonequilibrium Verwey transition in magnetite, Physical Review B, 93(5).
Sant'Ovaia, H., G. Marques, A. Santos, C. Gomes, and A. Rocha (2015), Magnetic susceptibility and isothermal remanent magnetization in human tissues: a study case, Biometals, 28(6), 951-958.
Witte, K., W. Bodnar, T. Mix, N. Schell, G. Fulda, T. G. Woodcock, and E. Burkel (2016), A detailed study on the transition from the blocked to the superparamagnetic state of reduction-precipitated iron oxide nanoparticles, Journal of Magnetism and Magnetic Materials, 403, 103-113.
Wu, M., J. S. Tse, and Y. M. Pan (2016), Electronic structures of greigite (Fe3S4): A hybrid functional study and prediction for a Verwey transition, Scientific Reports, 6.

Geomagnetism and the Earth's Dynamo

Ahn, H. S., T. Kidane, Y. Yamamoto, and Y. Otofuji (2016), Low geomagnetic field intensity in the Matuyama Chron: palaeomagnetic study of a lava sequence from Afar depression, East Africa, Geophysical Journal International, 204(1), 127-146.
Driscoll, P. E., and D. A. D. Evans (2016), Frequency of Proterozoic geomagnetic superchrons, Earth and Planetary Science Letters, 437, 9-14.
Lascu, I., J. M. Feinberg, J. A. Dorale, H. Cheng, and R. L. Edwards (2016), Age of the Laschamp excursion determined by U-Th dating of a speleothem geomagnetic record from North America, Geology, 44(2), 139-142.
Lifton, N. (2016), Implications of two Holocene time-dependent geomagnetic models for comogenic nuclide production rate scaling, Earth and Planetary Science Letters, 433, 257-268.
Opdyke, N. D., D. V. Kent, D. A. Foster, and K. Huang (2015), Paleomagnetism of Miocene volcanics on Sao Tome: Paleosecular variation at the Equator and a comparison to its latitudinal dependence over the last 5 Myr, Geochemistry Geophysics Geosystems, 16(11), 3870-3882.
O'Rourke, J. G., and D. J. Stevenson (2016), Powering Earth's dynamo with magnesium precipitation from the core, Nature, 529(7586), 387-+.
Sagnotti, L., P. Macri, and R. G. Lucchi (2016), Geomagnetic palaeosecular variation around 15 ka ago from NW Barents Sea cores (south of Svalbard), Geophysical Journal International, 204(2), 785-797.
Sagnotti, L., B. Giaccio, J. C. Liddicoat, S. Nomade, P. R. Renne, G. Scardia, and C. J. Sprain (2016), How fast was the Matuyama-Brunhes geomagnetic reversal? A new subcentennial record from the Sulmona Basin, central Italy, Geophysical Journal International, 204(2), 798-812.
Sprain, C. J., J. M. Feinberg, J. W. Geissman, B. Strauss, and M. C. Brown (2016), Paleointensity during periods of rapid reversal: A case study from the Middle Jurassic Shamrock batholith, western Nevada, Geological Society of America Bulletin, 128(1-2), 223-238.
Tarduno, J.A., M.K. Watkeys, T.N. Huffman, R.D. Cottrell1, E.G. Blackman, A. Wendt, C.A. Scribner, C.L. Wagner, 2015. Antiquity of the South Atlantic Anomaly and evidence for top-down control on the geodynamo, Nature Communications, 6:7865, DOI: 10.1038/ncomms8865.
Tarduno, J.A., R.D. Cottrell, W.J. Davis, F. Nimmo, R.K. Bono, 2015. A Hadean to Paleoarchean geodynamo recorded by single zircon crystals, Science, 349, 6247, 521-524.

High Pressure

Agarwal, A., A. Kontny, D. C. Srivastava, and R. O. Greiling (2016), Shock pressure estimates in target basalts of a pristine crater: A case study in the Lonar crater, India, Geological Society of America Bulletin, 128(1-2), 19-28.
Bezaeva, N. S., F. Demory, P. Rochette, R. A. Sadykov, J. Gattacceca, T. Gabriel, and Y. Quesnel (2015), The effect of hydrostatic pressure up to 1.61 GPa on the Morin transition of hematite-bearing rocks: Implications for planetary crustal magnetization, Geophysical Research Letters, 42(23).
Rochette, P., J. Gattacceca, B. Devouard, F. Moustard, N. S. Bezaeva, C. Cournede, and B. Scaillet (2015), Magnetic properties of tektites and other related impact glasses, Earth and Planetary Science

Letters, 432, 381-390.

Magnetic Fabrics and Anisotropy

Maffione, M., C. Hernandez-Moreno, M. C. Ghiglione, F. Speranza, D. J. J. van Hinsbergen, and E. Lodolo (2015), Constraints on deformation of the Southern Andes since the Cretaceous from anisotropy of magnetic susceptibility, Tectonophysics, 665, 236-250.

Petronis, M. S., A. R. Brister, V. Rapprich, B. V. de Vries, J. Lindline, and J. Misurec (2015), Emplacement history of the Trosky basanitic volcano (Czech Republic): paleomagnetic, rock magnetic, petrologic, and anisotropy of magnetic susceptibility evidence for lingering growth of a monogenetic volcano, Journal of Geosciences, 60(3), 129-147.

Renjith, A. R., M. A. Mamtani, and J. L. Urai (2016), Fabric analysis of quartzites with negative magnetic susceptibility - Does AMS provide information of SPO or CPO of quartz?, Journal of Structural Geology, 82, 48-59.

Soriano, C., E. Beamud, M. Garces, and M. H. Ort (2016), 'Anomalous' magnetic fabrics of dikes in the stable single domain/superparamagnetic threshold, Geophysical Journal International, 204(2), 1040-1059.

Mineral Physics

Aslibeiki, B., P. Kameli, and H. Salamati (2016), The effect of dipole-dipole interactions on coercivity, anisotropy constant, and blocking temperature of MnFe2O4 nanoparticles, Journal of Applied Physics, 119(6).

Gangwar, A., S. K. Alla, M. Srivastava, S. S. Meena, E. V. Prasadrao, R. K. Mandal, S. M. Yusuf, and N. K. Prasad (2016), Structural and magnetic characterization of Zr-substituted magnetite (ZrxFe3-xO4, 0 <= x <= 1), Journal of Magnetism and Magnetic Materials, 401, 559-566.

Gilks, D., et al. (2016), Atomic and electronic structure of twin growth defects in magnetite, Scientific Reports, 6.

Hevroni, A., B. Tsukerman, and G. Markovich (2015), Probing magnetization dynamics in individual magnetite nanocrystals using magnetoresistive scanning tunneling microscopy, Physical Review B, 92(22).

Prado, Y., et al. (2015), Enhancing the magnetic anisotropy of maghemite nanoparticles via the surface coordination of molecular complexes, Nature Communications, 6.

Taguchi, M., et al. (2015), Temperature Dependence of Magnetically Active Charge Excitations in Magnetite across the Verwey Transition, Physical Review Letters, 115(25).

Paleomagnetism

Babaahmadi, A., and G. Rosenbaum (2015), Kinematics of orocline-parallel faults in the Texas and Coffs Harbour oroclines (eastern Australia) and the role of flexural slip during oroclinal bending, Australian Journal of Earth Sciences, 62(8), 933-948.

Balmater, H. G., P. C. Manalo, D. V. Faustino-Eslava, K. L. Queano, C. B. Dimalanta, J. M. R. Guotana, N. T. Ramos, B. D. Payot, and G. P. Yumul (2015), Paleomagnetism of the Samar Ophiolite: Implications for the Cretaceous sub-equatorial position of the Philippine island arc, Tectonophysics, 664, 214-224.

Baltrunas, V., F. E. Maksimov, V. Y. Kuznetsov, B. Karmaza, and V. Katinas (2015), geochronology and palaeomagnetic records of the Snaigupele section in South Lithuania, Geochronometria, 42(1), 172-181.

Brooke-Barnett, S., and G. Rosenbaum (2015), Structure of the Texas Orocline beneath the sedimentary cover (southeast Queensland, Australia), Australian Journal of Earth Sciences, 62(4), 425-445.

Brown, L. L., and S. A. McEnroe (2015), 916 Ma Pole for southwestern Baltica: palaeomagnetism of the Bjerkreim-Sokndal layered intrusion, Rogaland Igneous Complex, southern Norway, Geophysical Journal International, 203(1), 567-587.

Chen, X. Y., J. L. Liu, S. T. Weng, Y. L. Kong, W. B. Wu, L. S. Zhang, and H. Y. Li (2016), Structural geometry and kinematics of the Ailao Shan shear zone: insights from integrated structural, microstructural, and fabric studies of the Yao Shan complex, Yunnan, Southwest China, International Geology Review, 58(7), 849-873.

D'Agrella, M. S., R. I. F. Trindade, M. V. B. Queiroz, V. T. Meira, L. Janikian, A. S. Ruiz, and F. Bispo-Santos (2016), Reassessment of Aguapei (Salto do Ceu) paleomagnetic pole, Amazonian Craton and implications for Proterozoic supercontinents, Precambrian Research, 272, 1-17.

Dembo, N., Y. Hamiel, and R. Granot (2015), Intraplate rotational deformation induced by faults, Journal of Geophysical Research-Solid Earth, 120(11), 7308-7321.

Eppelbaum, L., and Y. Katz (2015), Newly developed paleomagnetic map of the Easternmost Mediterranean joined with tectono-structural analysis unmask geodynamic history of this region, Open Geosciences, 7(1), 95-117.

Hamilton, E. M., R. D. Elmore, B. L. Weaver, S. Dulin, and J. Jackson (2016), Paleomagnetic and petrologic study of the age, origin, and significance of early and late Paleozoic events in the Long Mountain Granite, Wichita Mountains, Oklahoma, Geological Society of America Bulletin, 128(1-2), 187-202.

Hisarli, Z. M., M. C. Cinku, T. Ustaomer, M. Keskin, and N. Orbay (2016), Neotectonic deformation in the Eurasia-Arabia collision zone, the East Anatolian Plateau, E Turkey: evidence from palaeomagnetic study of Neogene-Quaternary volcanic rocks, International Journal of Earth Sciences, 105(1), 139-165.

Javadi, H. R., M. E. Ashtiani, B. Guest, A. Yassaghi, M. R. Ghassemi, M. Shahpasandzadeh, and A. Naeimi (2015), Tectonic reversal of the western Doruneh Fault System: Implications for Central Asian tectonics, Tectonics, 34(10), 2034-2051.

Koc, A., D. J. J. van Hinsbergen, N. Kaymakci, and C. G. Langereis (2016), Late Neogene oroclinal bending in the central Taurides: A record of terminal eastward subduction in southern Turkey?, Earth and Planetary Science Letters, 434, 75-90.

Li, Y. X., X. X. Zhao, L. Jovane, K. E. Petronotis, Z. Gong, and S. Y. Xie (2015), Paleomagnetic constraints on the tectonic evolution of the Costa Rican subduction zone: New results from sedimentary successions of IODP drill sites from the Cocos Ridge, Geochemistry Geophysics Geosystems, 16(12), 4479-4493.

Ma, Y. M., T. S. Yang, W. W. Bian, J. J. Jin, S. H. Zhang, H. C. Wu, and H. Y. Li (2016), Early Cretaceous paleomagnetic and geochronologic results from the Tethyan Himalaya: Insights into the Neotethyan paleogeography and the India-Asia collision, Scientific Reports, 6.

Mankinen, E. A., and C. M. Wentworth (2016), Paleomagnetic record determined in cores from deep research wells in the Quaternary Santa Clara basin, California, Geosphere, 12(1), 35-57.

McCarthy, W., R. J. Reavy, C. T. Stevenson, and M. S. Petronis (2015), Late Caledonian transpression and the structural controls on pluton construction; new insights from the Omey Pluton, western Ireland, Earth and Environmental Science Transactions of the Royal Society of Edinburgh, 106(1), 11-28.

Morris, A., and M. Maffione (2016), Is the Troodos ophiolite (Cyprus) a complete, transform fault-bounded Neotethyan ridge segment?, Geology, 44(3), 199-202.

Morris, A., A. H. F. Robertson, M. W. Anderson, and E. Hodgson (2016), Did the Kyrenia Range of northern Cyprus rotate with the Troodos-Hatay microplate during the tectonic evolution of the eastern Mediterranean?, International Journal of Earth Sciences, 105(1), 399-415.

Oksum, E., Z. M. Hisarli, M. C. Cinku, T. Ustaomer, and N. Orbay (2015), New paleomagnetic results from Ordovician sedimentary rocks from NW Anatolia: Tectonic implications for the paleolatitudinal position of the Istanbul Terrane, Tectonophysics, 664, 14-30.

Pastor-Galan, D., B. Ursem, P. A. Meere, and C. Langereis (2015), Extending the Cantabrian Orocline to two continents (from Gondwana to Laurussia). Paleomagnetism from South Ireland, Earth and Planetary Science Letters, 432, 223-231.

Peng, C., L. F. Xue, M. Zhu, Y. Chai, and W. Y. Liu (2016), The location and evolution of the tectonic boundary between the Paleoproterozoic Jiao-Liao-Ji Belt and the Longgang Block, northeast China, Precambrian Research, 272, 18-38.

Polteau, S., B. W. H. Hendriks, S. Planke, M. Ganerod, F. Corfu, J. I. Faleide, I. Midtkandal, H. S. Svensen, and R. Myklebust (2016), The Early Cretaceous Barents Sea Sill Complex: Distribution, Ar-40/Ar-39 geochronology, and implications for carbon gas formation, Palaeogeography Palaeoclimatology Palaeoecology, 441, 83-95.

Richter, F., C. Lana, G. Stevens, I. Buick, A. C. Pedrosa-Soares, F. F. Alkmim, and K. Cutts (2016), Sedimentation, metamorphism and granite generation in a back-arc region: Records from the Ediacaran Nova Venecia Complex (Aracuai Orogen, Southeastern Bra-

zil), Precambrian Research, 272, 78-100.
Sandjo, A. F. Y., T. Njanko, E. Njonfang, E. Errami, P. Rochette, and E. Fozing (2016), Transpressional granite-emplacement model: Structural and magnetic study of the Pan-African Bandja granitic pluton (West Cameroon), Journal of Earth System Science, 125(1), 179-202.
Saroli, M., M. Moro, F. Florindo, M. Lancia, P. C. Lurcock, and J. Dinares-Turell (2015), Paleomagnetic dating of tectonically influenced Plio-Quaternary fan-system deposits from the Apennines (Italy), Annals of Geophysics, 58.
Shaanan, U., G. Rosenbaum, S. Pisarevsky, and F. Speranza (2015), Paleomagnetic data from the New England Orogen (eastern Australia) and implications for oroclinal bending, Tectonophysics, 664, 182-190.
Shi, W., S. W. Dong, Y. Q. Zhang, and S. Q. Huang (2015), The typical large-scale superposed folds in the central South China: Implications for Mesozoic intracontinental deformation of the South China Block, Tectonophysics, 664, 50-66.
Swanson-Hysell, N. L., T. M. Kilian, and R. E. Hanson (2015), A new grand mean palaeomagnetic pole for the 1.11 Ga Umkondo large igneous province with implications for palaeogeography and the geomagnetic field, Geophysical Journal International, 203(3), 2237-2247.
Symons, D. T. A., P. J. A. McCausland, K. Kawasaki, and C. J. R. Hart (2015), Post-Triassic para-autochthoneity of the Yukon-Tanana Terrane: paleomagnetism of the Early Cretaceous Quiet Lake batholith, Geophysical Journal International, 203(1), 312-326.
Torres-Carrillo, X. G., L. A. Delgado-Argote, H. Bohnel, R. S. Molina-Garza, and B. Weber (2016), Palaeomagnetic assessment of plutons from the southern Peninsular Ranges batholith and the Jurassic Vizcaino igneous suites, Baja California, Mexico, International Geology Review, 58(4), 489-509.
Tsuchiyama, Y., H. Zaman, S. Sotham, Y. Samuth, E. Sato, H. S. Ahn, K. Uno, K. Tsumura, M. Miki, and Y. Otofuji (2016), Paleomagnetism of Late Jurassic to Early Cretaceous red beds from the Cardamom Mountains, southwestern Cambodia: Tectonic deformation of the Indochina Peninsula, Earth and Planetary Science Letters, 434, 274-288.
Xiao, W. J. (2015), New paleomagnetic data confirm a dual-collision process in the Himalayas, National Science Review, 2(4), 395-396.
Yu, S., S. Z. Li, S. J. Zhao, H. H. Cao, and Y. H. Suo (2015), Long history of a Grenville orogen relic - The North Qinling terrane: Evolution of the Qinling orogenic belt from Rodinia to Gondwana, Precambrian Research, 271, 98-117.
Zhang, T., W. X. Han, X. M. Fang, W. L. Zhang, C. H. Song, and M. D. Yan (2016), Intensified tectonic deformation and uplift of the Altyn Tagh range recorded by rock magnetism and growth strata studies of the western Qaidam Basin, NE Tibetan Plateau, Global and Planetary Change, 137, 54-68.

Prospecting and Surveying

Azeez, K. K. A., K. Veeraswamy, A. K. Gupta, N. Babu, S. Chandrapuri, and T. Harinarayana (2015), The electrical resistivity structure of lithosphere across the Dharwar craton nucleus and Coorg block of South Indian shield: Evidence of collision and modified and preserved lithosphere, Journal of Geophysical Research-Solid Earth, 120(10), 6698-6721.
Hartmann, L. A., J. F. Savian, and W. R. Lopes (2016), Airborne geophysical characterization of geotectonic relationships in the southern Ribeira Belt, Luis Alves Craton, and northern Dom Feliciano Belt, Brazilian Shield, International Geology Review, 58(4), 471-488.
Hendrickson, M. D. (2016), Geologic interpretation of aeromagnetic and chemical data from the Oaks Belt, Wabigoon subprovince, Minnesota: implications for Au-rich VMS deposit exploration, Canadian Journal of Earth Sciences, 53(2), 176-188.
Kapinos, G., U. Weckmann, M. Jegen-Kulcsar, N. Meqbel, A. Neska, T. T. Katjiuongua, S. Hoelz, and O. Ritter (2016), Electrical resistivity image of the South Atlantic continental margin derived from onshore and offshore magnetotelluric data, Geophysical Research Letters, 43(1), 154-160.
Oskooi, B., M. Mirzaei, B. Mohammadi, M. Mohammadzadeh-Moghaddam, and F. Ghadimi (2016), Integrated interpretation of the magnetotelluric and magnetic data from Mahallat geothermal field, Iran, Studia Geophysica Et Geodaetica, 60(1), 141-161.

Spectroscopy

Banerjee, S., S. Mondal, P. P. Chakraborty, and S. S. Meena (2015), Distinctive compositional characteristics and evolutionary trend of Precambrian glaucony: Example from Bhalukona Formation, Chhattisgarh basin, India, Precambrian Research, 271, 33-48.
Berger, J. A., et al. (2016), A global Mars dust composition refined by the Alpha-Particle X-ray Spectrometer in Gale Crater, Geophysical Research Letters, 43(1), 67-75.
Surtees, A. P. H., G. T. Swindles, I. P. Savov, I. J. Scowen, H. G. M. Edwards, and T. Munshi (2016), Raman spectroscopy for the discrimination of tephras from the Hekla eruptions of AD 1510 and 1947, Holocene, 26(3), 432-438.
Van Ranst, E., E. Padmanabhan, R. E. Vandenberghe, E. De Grave, and F. Mees (2016), Yellowing of a Red South African Kandiudult, Studied by Means of Mossbauer Spectroscopy, Soil Science, 181(2), 75-81.

Statistics, Computing and Modelling

Chave, A. D. (2015), A note about Gaussian statistics on a sphere, Geophysical Journal International, 203(2), 893-895.
Dobosz, B., R. Krzyminiewski, M. Koralewski, and M. Halupka-Bryl (2016), Computer enhancement of ESR spectra of magnetite nanoparticles, Journal of Magnetism and Magnetic Materials, 407, 114-121.
Khokhlov, A., and G. Hulot (2016), Principal component analysis of palaeomagnetic directions: converting a Maximum Angular Deviation (MAD) into an alpha(95) angle, Geophysical Journal International, 204(1), 274-291.
Paine, J., R. De Ritis, G. Ventura, M. Longo, D. Ravat, F. Speranza, and M. Chiappini (2016), Inverse modelling of the reversely magnetized, shallow plumbing system hosting oil reservoirs of the Auca Mahuida volcano (Payeina retroarc, Neuquen Basin, Argentina), Geophysical Journal International, 204(2), 852-867.

Stratigraphy

Bazhenov, M. L., N. M. Levashova, J. G. Meert, I. V. Golovanova, K. N. Danukalov, and N. M. Fedorov (2016), Late Ediacaran magnetostratigraphy of Baltica: Evidence for Magnetic Field Hyperactivity?, Earth and Planetary Science Letters, 435, 124-135.
Duan, Z. Q., Q. S. Liu, X. F. Shi, Z. Q. Yao, J. X. Liu, and K. Su (2016), Reconstruction of high-resolution magnetostratigraphy of the Changjiang (Yangtze) River Delta, China, Geophysical Journal International, 204(2), 948-960.
Plasota, T., J. Nawrocki, and I. Walaszczyk (2015), Magnetostratigraphy of the Campanian/Maastrichtian boundary succession from the Middle Vistula River section, central Poland, Geological Quarterly, 59(4), 831-842.
Shatsillo, A. V., N. B. Kuznetsov, V. E. Pavlov, M. A. Fedonkin, N. S. Priyatkina, S. G. Serov, and S. V. Rudko (2015), The first magnetostratigraphic data on the stratotype of the Lopata Formation, Northeastern Yenisei Ridge: Problems of its age and paleogeography of the Siberian Platform at the Proterozoic-Phanerozoic boundary, Doklady Earth Sciences, 465(2), 1211-1214.

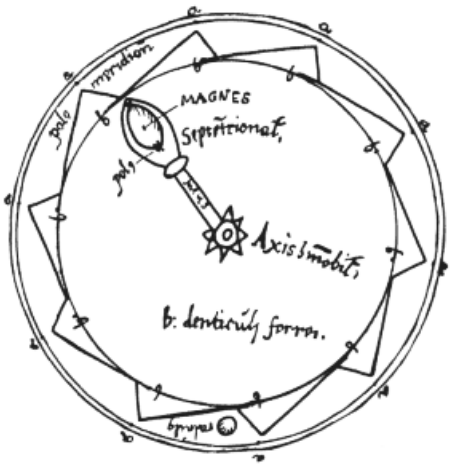

cont'd. from pg. 1...

case, the number of characteristic X-ray photons reveals the concentration of each element. Because this process involves inner-shell orbital electrons, XRF is suitable for identifying elements only, not isotopes or chemical bonds. The IRM's new instrument is an ED-pXRF with rapid measurements (30-60 s) that are entirely non-destructive, so no material is lost or damaged during the course of an analysis.

Features

Specifically, the IRM instrument is a Thermo Scientific Niton XL3t 950 GOLDD+ (Geometrically Optimized Large-Area Drift Detector) ED-XRF analyzer. The instrument is portable, but it is set up primarily for benchtop operation for IRM visitors. It has a miniaturized 50-kV, 2-W, silver-anode X-ray tube as an excitation source (not the radioactive isotopes found in many older models). The X-ray detector is the latest generation of silicon drift detector (SDD), which is up to ten times faster than older Si PN-diode detectors and up to three times faster than first-generation SDDs. The circular analytical window is 10 mm across, and the incident X-ray beam is about 8 mm in diameter. A built-in collimator can, if one chooses, limit the beam diameter to 3 mm, thereby reducing the analyzed area on a specimen from 50 to 7 mm^2 (an area 85% smaller); however, collimation should be used judiciously, as the number of incident X-rays is reduced commensurately, yielding higher measurement uncertainties and detection limits. A camera inside the instrument can aid in positioning small specimens in the collimated X-ray beam. While the pXRF is notably smaller than the laboratory-based XRF instruments that many of us are familiar with, equally important is the development and refinement of the instrument's data correction algorithms that turn X-ray intensities into element concentrations.

Modes of Operation

Our instrument has two principal analytical modes: Soils and Mining. The "Mining" mode was initially developed for exploration geologists to measure elements of interest to the mining industry in silicate rocks, whereas the "Soils" mode was originally intended for conducting environmental surveys of soil contaminants, where elements of interest might fall between their natural abundances in Earth's crust and the much higher concentrations encountered at contaminated sites. Thus, these modes differ in several important ways. For example, the pre-set list of measured elements differs between modes. The "Soils" mode measures the concentrations of 33 elements: Ag, As, Au, Ba, Ca, Cd, Co, Cr, Cs, Cu, Fe, Hg, K, Mn, Mo, Ni, Pb, Pd, Rb, S, Sb, Sc, Se, Sn, Sr, Te, Ti, Th, U, V, W, Zn, and Zr. The "Mining" mode measures 42 elements: Ag, Al, As, Au, Ba, Bi, Ca, Cd, Ce, Cl, Co, Cr, Cu, Fe, Hf, K, La, Mg, Mn, Mo, Nb, Nd, Ni, P, Pb, Pd, Pr, Rb, Re, S, Sb, Se, Si, Sn, Sr, Ta, Ti, V, W, Y, Zn, and Zr. Earlier XRF instruments required helium purging or vacuum pumps to analyze light elements ($Z < 17$), but this is no longer necessary with the "Mining" mode and the latest generation of SDD technology. Different sets of elements are measured using a sequence of X-ray "filters" (up to four in "Mining" mode, up to three in "Soils" mode) that improve sensitivity for select portions of the energy spectrum. The instrument automatically changes these built-in filters during an analysis so that the low, middle, and high end of a specimen's X-ray spectrum is sequentially enhanced.

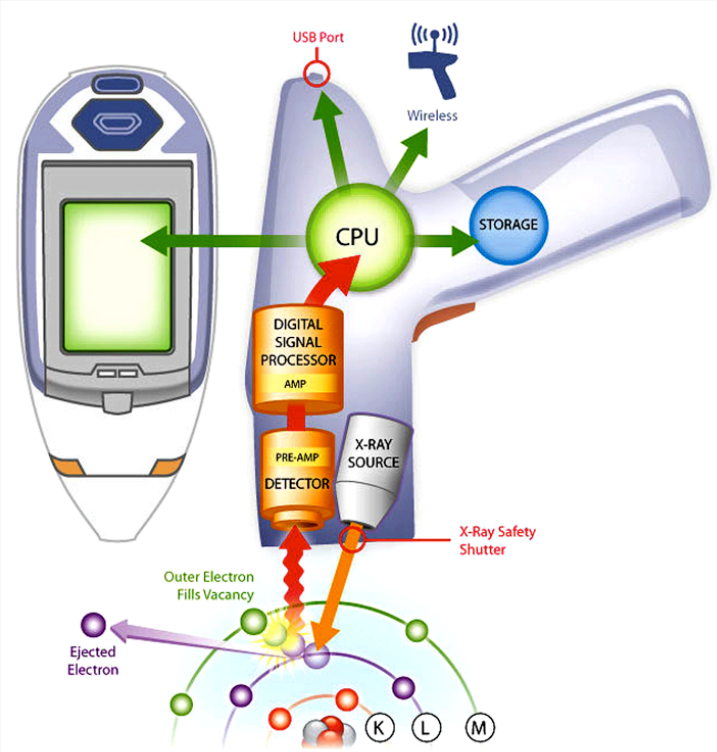

Schematic diagram of the p-XRF from Thermo-Scientific.

Conversion

Another difference between these two analytical modes involves the algorithms used to convert raw X-ray intensity measurements into element concentrations. The relationship between an element's characteristic X-ray emission intensity and its concentration within a material is not straightforward. Various phenomena, including the excitation of lighter elements by characteristic X-rays from heavier elements, occur within a material, altering the measured intensities. The two operational modes use different correction approaches to convert X-ray counts into first approximations of the elements' concentrations. The "Soils" mode uses a simpler "Compton normalization" approach. The lower the mean atomic number of a material, the greater the intensity of the incoherently scattered X-rays (the Compton peak). This relationship also applies, albeit to a lesser degree, to the coherently scattered X-rays (the Raleigh peak). The ratio of the two peaks (Compton/Raleigh) is proportional to a specimen's mean atomic number and, in turn, its average composition. Additionally, this correction approach uses the Compton and Raleigh peaks as a means to compensate for a specimen's morphology, texture, density, and other effects. In contrast, the "Mining" mode applies the more calculation-intensive "fundamental parameters

(FP)" approach. FP correction involves iterative corrections to the measured X-rays using a mathematical description of instrument conditions (e.g., X-ray tube emissions, detector efficiency) and instrument-independent parameters for each element (e.g., X-ray fluorescence intensities, absorption coefficients, absorption edges). These parameters are brought together in an algorithm that solves a range of nonlinear equations describing the relationships between measured X-ray intensities and accurate element concentrations.

Calibration

Both correction approaches also use responses to standards or reference materials as a means to calibrate the data and return quantitative results. The factory-set "internal" calibrations are intended to remain stable over long periods and accurate over a range of materials and elemental concentrations. For example, for environmental surveying, the calibration must account for materials with element concentrations which fall at the two extreme ends of the spectrum: loess deposits in which cadmium occurs near or below the detections limit may constitute one extreme, whereas contaminated river sediments that possess much higher concentrations may lie at the opposite end. The intention is that these "internal" calibrations can be used in various tasks and acquire suitable data. Applications such as obsidian characterization, in which trace elements and the overall compositions fall within narrow ranges, tend to reveal the limitations of factory-set calibrations. In such applications, analyses of geochemical standards or other reference materials are commonly needed to "fine tune" the factory-set calibrations using linear regression in order to yield the most accurate measurements. The IRM maintains an impressive suite of geochemical standards for granular and solid materials to aid with most geological applications.

Specimen Limitations

XRF is a largely surficial analytical technique, but it is important to note that X-rays from different elements escape a specimen from different depths. As a general rule, the greater the atomic number, the greater the depth of X-ray penetration in a specimen. The characteristic X-rays emitted from, for example, iron (6.4 keV) escape from the top few micrometers of the specimen surface, whereas zirconium X-rays (15.8 keV) can escape from a few hundred micrometers deep. Energetic barium X-rays escape from a centimeter or more deep, depending on the material. In thick, homogenous specimens, this difference in measurement depth has little effect. If specimens are thin, however, it can affect the spectrum in various ways, depending on the specimen thickness and elements of interest. Hence, for the best data correction, a specimen should be sufficiently thick to completely absorb the incident X-ray beam. For many rocks and minerals, only a few millimeters of material is sufficiently thick. For a light-element matrix such as, for example, coal, a few centimeters of material is needed. Additionally, because characteristic X-rays from light elements have lower energies, they are more easily reabsorbed within the specimen and, in turn, are more sensitive to irregular specimen morphology, surface contamination, and other effects. Consequently, analyzing for Zr, Sr, and Rb in a specimen of obsidian that is 1-cm thick and has a clean, flat surface will yield ideal results. As a specimen becomes smaller, thinner, or less homogeneous and/or the elements of interest become lighter, an understanding of the X-ray interactions becomes more important.

Detection Limits

The minimum detection limits also vary by element, concentration, material, and measurement time. For favorable elements like Zr, Sr, and Rb, detection limits circa 1-2 ppm in a silicate matrix are often attainable in only 30 seconds. Detection limits for other elements, especially lighter ones, will be higher and/or take longer.

Safety and User Friendliness

For the safety of visiting researchers, the instrument is mounted in a test stand that allows hands-free measurements. The pXRF is fully shielded to protect operator from primary or scattered radiation, and a computer operates the instrument remotely for additional safety.

Our particular test stand is optimized for one-inch round drill cores, similarly sized cups are available for finely powdered materials, or smaller specimens. Larger specimens can either be accommodated by the stand or measured with the instrument in handheld mode.

The p-XRF and the IRM Database

All measurements are downloaded from the instrument via the computer and exported to an Excel file and will ultimately be stored in the IRM Database along with other data generated by a user. The goal is for users to be able to generate bivariate plots with combinations of element concentrations or ratios and magnetic properties, or composition as a function of stratigraphy. For the time being, however, users will be able to export a spreadsheet and plot their data using their favorite software.

Having non-destructive XRF available at the IRM will allow future visitors to correlate magnetic and elemental data from the very same specimens, double-check that specimens originated from the same geological facies or stratum, collect independent data for petrological identifications, and a variety of other yet-to-be-discovered applications. We hope that this instrument will contribute to rock magnetic research across a variety of fields. For further details on XRF analysis, interested readers are referred to Beckhoff et al. (2006).

References:

Beckhoff, B., Kanngießer, B., Langhoff, N., Wedell, R., Wolff, H. 2006. Handbook of Practical X-Ray Fluorescence Analysis, Springer, ISBN 3- 540-28603-9.

Frahm, E. 2014. Characterizing Obsidian Sources with Portable XRF: Accuracy, Reproducibility, and Field Relationships in a Case Study from Armenia. Journal

of Archaeological Science 49:105-125.
Frahm, E., Schmidt, B., Gasparyan, B., Yeritsyan, B., Karapetian, S., Meliksetian, Kh., Adler, D.S. 2014. Ten Seconds in the Field: Rapid Armenian Obsidian Sourcing with Portable XRF to Inform Excavations and Surveys. Journal of Archaeological Science 41:333-348.
Frahm, E., Feinberg, J.M., Schmidt-Magee, B.A., Wilkinson, K.N., Gasparyan, B., Yeritsyan, B., and Adler, D.S., 2016. Middle Paleolithic Lithic Procurement Behaviors at Lusakert Cave 1, Hrazden Valley, Armenia. Journal of Human Evolution, 91, 73-92.
Funk, J.A:, von Dobeneck, T., von, Reitz, A., 2004. Integrated rock magnetic and geochemical quantification of redoxmorphic iron mineral diagenesis in Late Quaternary sediments from the equatorial Atlantic: In: Wefer, G., Mulitza, S., Ratmeyer, V. (eds.): The South Atlantic in the Late Quaternary, Springer, 237-260
Funk, J.A:, von Dobeneck, T., von, Wagner, T., Kasten, S., 2004. Late Quaternary sedimentation and early diagenesis in the equatorial Atlantic Ocean: pattern, trends, and processes deduced from rock magnetic and geochemical records: In: Wefer, G., Mulitza, S., Ratmeyer, V. (eds.): The South Atlantic in the Late Quaternary, Springer, 461-497
Gazley, M.F., Duclaux, G., Fisher, L.A., Tutt, C.M., Latham, A.R., Hough R.M., De Beer, S.J., and Taylor, M.D., 2015, A comprehensive approach to understanding ore deposits using portable X-ray fluorescence (pXRF) data at the Plutonic Gold Mine, Western Australia. Geochemistry-Exploration Environment Analysis, 15 (2-3), 113-124.
Jamieson, H.,E., Walker, S.R., and Parsons, M.B., 2015, Mineralogical characterization of mine waste, Applied Geochemistry, 57, 85-105.
Kuhlmann, H., Freudenthal, T., Helmke, P., and Meggers, H., 2004. Reconstruction of paleoceanography off NW Africa for the last 40,000 years: influence of local and regional factors on sediment accumulation. Marine Geology, 207(1-4): 209-234.
Kuhlmann, H., Meggers, H., Freudenthal, T., Wefer, G., 2004. The transition of the monsoonal and the N Atlantic climate system off NW Africa during the Holocene. Geophysical Research Letters 31(22): L22204
Lamy, F., Kaiser, J., Ninnemann, U., Hebbeln, D., Arz, H.W. & Stoner, J., 2004. Antarctic timing of surface water changes off Chile and Patagonian ice-sheet response. Science, 304: 1959-1962
Luterbacher, H. P., Ali, J. R., Brinkhuis, H., Gradstein, F. M., Hooker, J. J., Monechi, S., Ogg,, J. G., Powell, J., Röhl, U., Sanfilippo, A., and B. Schmitz, 2004. The Paleogene period. In: Felix Gradstein, F, Ogg, J G, and A Smith (eds.): A Geologic Time Scale 2004, Cambridge University Press 2004.
Martin Peinado, F., Ruano, S.M., Gonzalez, M.G.B., and Molina, C.E., 2010. A rapid field procedure for screening trace elements in polluted soil using portable X-ray fluorescence (pXRF), Geoderma, 159 (1-2), 76-82.
Meijers, M.J.M., Strauss, B.E., Öxkaptan, M., Feinberg, J.M., Mulch, A., Whitney, D., and Kaymakci, N., 2016. Age and paleoenvironmental reconstruction of partially remagnetized lacustrine sedimentary rocks (Oligocene Aktoprak basin, Central Anatolia, Turkey). Geochemistry, Geophysics, Geosystems, 17, doi: 10.1002/2015GC006209.
Röhl, U., Brinkhuis, H., Fuller, M., 2004. On the search for the Paleocene/Eocene boundary in the Southern Ocean: exploring ODP Leg 189 Holes 1171D and 1172D.- In: Exon, N F, Malone, M, and Kennett, J P, eds., The Cenozoic Southern Ocean and Climate Change between Australia and Antarctica. American Geophysical Union, Geophysical Monograph Series, 181: 113-126
Röhl, U., Brinkhuis, H., Fuller, M., Schellenberg, S. A., Stickley, C. E., Williams, G. L., 2004. Cyclostratigraphy of middle and late Eocene sediments drilled on the East Tasman Plateau (Site 1172).- In Exon, NF, Malone, M, and Kennett, JP (Eds.), Climate evolution in the Southern Ocean and Australia's Cenozoic flight northward from Antarctica. American Geophysical Union, Geophysical Monograph Series, 181: 127-152

Obsidian artifacts created by Neanderthals ready for pXRF measurement.

Important Deadlines!!!

Summer School in Rock Magnetism: April 30th

and

Visiting Fellow Application: April 30th

Find details at
https://irm.umn.edu

University of Minnesota
291 Shepherd Laboratories
100 Union Street S. E.
Minneapolis, MN 55455-0128
phone: (612) 624-5274
fax: (612) 625-7502
e-mail: irm@umn.edu
www.irm.umn.edu

Nonprofit Org.
U.S Postage
PAID
Twin Cities, MN
Permit No. 90155

The IRM Quarterly

The *Institute for Rock Magnetism* is dedicated to providing state-of-the-art facilities and technical expertise free of charge to any interested researcher who applies and is accepted as a Visiting Fellow. Short proposals are accepted semi-annually in spring and fall for work to be done in a 10-day period during the following half year. Shorter, less formal visits are arranged on an individual basis through the Facilities Manager.

The *IRM* staff consists of **Subir Banerjee**, Professor/Founding Director; **Bruce Moskowitz**, Professor/Director; **Joshua Feinberg**, Assistant Professor/Associate Director; **Mike Jackson, Peat Sølheid** and **Dario Bilardello**, Staff Scientists.

Funding for the *IRM* is provided by the **National Science Foundation**, the **W. M. Keck Foundation**, and the **University of Minnesota**.

The *IRM Quarterly* is published four times a year by the staff of the *IRM*. If you or someone you know would like to be on our mailing list, if you have something you would like to contribute (*e.g.*, titles plus abstracts of papers in press), or if you have any suggestions to improve the newsletter, please notify the editor:

Dario Bilardello
Institute for Rock Magnetism
University of Minnesota
291 Shepherd Laboratories
100 Union Street S. E.
Minneapolis, MN 55455-0128
phone: (612) 624-5274
fax: (612) 625-7502
e-mail: dario@umn.edu
www.irm.umn.edu

UNIVERSITY OF MINNESOTA